Eurographics Workshop on Visual Computing for Biology and Medicine (2017)
S. Bruckner, A. Hennemuth, and B. Kainz (Editors)

Exploration of Interventricular Septum Motion in Multi-Cycle Cardiac MRI

Lennart Tautz[†1], Markus Hüllebrand[2], Michael Steinmetz[3], Dirk Voit[4], Jens Frahm[4], Anja Hennemuth[1]

[1]Charité - Universitätsmedizin Berlin, Institute for Cardiovascular Computer-Assisted Medicine, Germany
[2]Fraunhofer MEVIS, Germany
[3]Universitätsmedizin Göttingen, Germany
[4]Biomedizinische NMR Forschungs GmbH at the MPI for Biophysical Chemistry, Germany

Abstract

Function of the heart, including interventricular septum motion, is influenced by respiration and contraction of the heart muscle. Recent real-time magnetic resonance imaging (MRI) can acquire multi-cycle cardiac data, which enables the analysis of the variation between heart cycles depending on factors such as physical stress or changes in respiration. There are no normal values for this variation in the literature, and there are no established tools for the analysis and exploration of such multi-cycle data available. We propose an analysis and exploration concept that automatically segments the left and right ventricle, extracts motion parameters and allows to interactively explore the results. We tested the concept using nine real-time MRI data sets, including one subject under increasing stress levels and one subject performing a breathing maneuver. All data sets could be automatically processed and then explored successfully, suggesting that our approach can robustly quantify and explore septum thickness in real-time MRI data.

CCS Concepts

•***Human-centered computing*** → ***Visual analytics;*** •***Computing methodologies*** → ***Image segmentation;***

1. Introduction

The function of the human heart is modulated by the interaction of the left and right ventricles (LV, RV) with respiration. Depending on load and pressure in the ventricles, the interventricular septum (IVS), which separates the two heart chambers (Figure 1), changes its shape and position in response to both the cardiac and respiratory cycle. While the high-frequency cardiac cycle affects the septum primarily by contraction of the ventricles, the respiratory cycle with its much lower frequency changes the position of the heart as a whole and modulates the distribution of the blood in the body. The latter periodically shifts blood from the systemic to the pulmonary circulation, which again affects the shape of the interventricular septum. This complex interaction may be further influenced by pharmacological stress or physical exercise or other active changes in breathing.

Heart function can be characterized by deriving metrics from dynamic magnetic resonance imaging (MRI) recordings. Such metrics range from global parameters such as LV blood pool (LVBP) volume to regional indices such as LV myocardium (LVM) thickness or myocardial strain. Typically, such parameters are derived for single, representative heart cycles obtained by echocardiography (ultrasound, US) or MRI. However, recent advances in real-time MRI now allow for acquisitions of successive multi-cycle data of the heart (Uecker et al. [UZV*10]). So far, there are no normal values on the variation of most of the functional parameters over multiple heartbeats, or in response to physiological alterations or physical stress. In this work, we propose an approach for the analysis and exploration of IVS motion over multiple heart cycles using real-time cardiac MRI. Our aim is to provide a means of analysis of multi-cycle variation and stress-related changes that can robustly and precisely quantify functional parameters from real-time MRI data. We propose to automatically segment the left and right ventricle, then extract landmarks describing IVS motion from the segmentations and explore the derived motion parameters in an interactive step centered on a parallel coordinates display and temporally synchronized viewers.

2. Related Work

Historically, the behavior of the IVS has been assessed by echocardiography (Diamond et al. [DDH*71], Zee-Cheng et al. [ZCG85]) or cine MRI (Roeleveld et al. [RMF*05]). Whereas US techniques represent true single-cycle acquisitions, conventional ECG-synchronized cine MRI techniques merge data from multiple heartbeats to generate a single synthetic cardiac cycle. Therefore, real-

† lennart.tautz@charite.de

DOI: 10.2312/vcbm.20171251

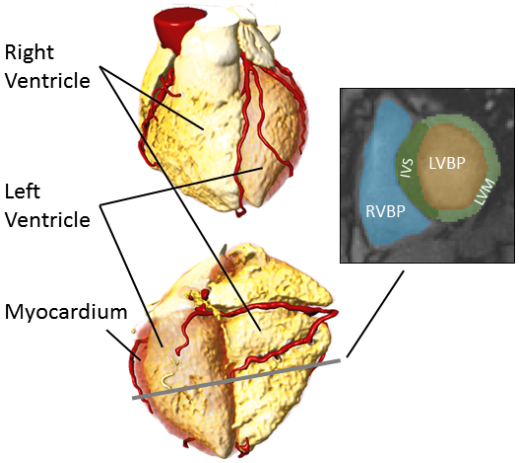

Figure 1: *Left top and bottom: 3D views of the heart with all chambers, with indication where a short-axis slice is located. Right: Short-axis slice with relevant regions (RVBP: RV blood pool, LVBP: LV blood pool, LVM: LV myocardium, IVS: interventricular septum).*

time MRI was proposed to acquire and explore multi-cyclic image data (Francone et al. [FDKB05]). Major advances now offer real-time MRI acquisitions and reconstructions, which directly monitor multiple cardiac cycles with high temporal resolution (e.g., 20 ms), and therefore provide immediate access to functional variability across cycles in the healthy and diseased heart (Uecker et al. [UZV*10], Feng et al. [FAC*16]). Preliminary work has focused on the quantification of IVS motion in different heart cycles (Tautz et al. [TFO*16a, TFO*16b], Chitiboi et al. [CRF*17]) and proposed to use color-coded parameter maps and parallel coordinates for visualization, but has only dealt in a limited way with the question of how the data can be presented and explored.

Visualization of multi-variate or multi-parameter results is a common problem when dealing with complex medical or biological data. One way to explore this type of data are parallel coordinates (Inselberg [Ins85]), where several parameters that are associated with each other are plotted in parallel and connected by lines. To visualize the association of parameters with time or spatial location, a number of mapping techniques have been proposed. Vinegoni et al. [VFR*12] proposed bull's eye and cylindrical projections to associate parameters with different heart regions. Breeuwer [Bre02] introduced the perfusogram, which plots time against spatial location. Andrienko et al. [AABW12] used time-trajectory maps to visualize eye movement that encode time, spatial location and frequency of occurrence. Oeltze et al. [ODH*07] used color-coded, time-varying plots to visualize cardiac perfusion parameters. The approaches in the survey given by Preim et al. [POM*09] include color-coded height fields for multi-parameter visualization. TomTec's 2D Cardiac Performance Analysis MR software offers color-coded maps overlaid over the myocardium to relate strain behavior in space and time.

These techniques are well-suited for multi-parameter display, but hampered in the visualization of a parameter which depends on two temporal dimensions (cardiac and respiratory phase). There is no integrated concept on how such data can be explored interactively, which we deem critical for the assessment of real-time cardiac parameters.

Segmentation of the right ventricle has only recently gained increased attention. Petitjean et al. [PD11] reviewed segmentation algorithms for both heart large chambers, and noted the small number of publications on right ventricle segmentation, the complexity of the task and the lack of representative and comparable evaluation data. The authors subsequently organized a segmentation challenge at MICCAI 2012 (Petitjean et al. [PZB*15]), which provided a common set of cine MRI data and evaluation metrics. Seven groups participated in the challenge, with a wide range of approaches. Four of the proposed methods required limited input by the user, the others were fully automatic. The majority of methods proposed to incorporate prior knowledge from training data in the form of multi-atlas registration or shape models. More recent publications from Luo et al. [LAW*16], Tran [Tra16] and Wang et al. [WML*17] focused on applying deep learning techniques to the data set provided by the MICCAI challenge. Chitiboi et al. [CHT*14, CHT*15] and Zöhrer et al. [ZHC*17] noted that contrast and other image characteristics such as edge sharpness differ considerably between conventional cine MRI and real-time MRI. To our knowledge, there are no publications concerning the segmentation of the right ventricle in real-time MRI data.

3. Methods

Our processing pipeline consists of the segmentation of both ventricles, automatic quantification of the septum thickness and an interactive exploration phase. We tested this approach with a small number of real-time MRI datasets.

3.1. Data

Real-time cardiac MRI (Uecker et al. [UZV*10]) is an image acquisition and reconstruction technique with high temporal resolution and contrast comparable to conventional cine acquisitions. Images are acquired without triggering (ECG or breathing) under normal respiration, which means the acquired image series shows different respiration states and also includes heart cycles that normally would be discarded, such as arrhythmic cycles. Major challenges in processing such data are the variation of tissue contrast over time, weak contrast between LVBP and LVM especially in systolic (contracted) phases, and the amount of data to be processed.

We chose ten 2D multi-cycle short-axis real-time MRI acquisitions of three healthy subjects to test our approach (Table 1). These acquisitions show slices as described in Figure 1, showing the complete myocardium through all cycles. All datasets had an in-plane resolution of 1.6 mm x 1.6 mm and a slice thickness of 6 mm. For one subject, the acquisitions include different ergometer-induced stress levels. One subject performed a Valsalva maneuver (i.e., pressure on the upper thorax during a 10 s breathhold, Gorlin et al. [GKS57]). The datasets show a varying number of heart cycles, caused by different acquisition lengths and physiological conditions. The images were acquired on a Siemens Prisma fit and a Siemens Skyra both operating at 3 T.

Subject	Condition	Temporal resolution [ms]	Heart cycles
P1	a (Normal)	33.3	6
	b (Normal)	33.3	5
P2	a (Normal)	33.3	8
	b (Normal)	25.0	7
P3	a (Normal)	33.3	3
	b (Stress 50W)	33.3	5
	c (Stress 70W)	33.3	6
	d (Stress 90W)	33.3	7
	e (Stress 100W)	33.3	9
P4	Valsalva	33.3	36

Table 1: *Analyzed datasets: three subjects underwent subsequent examinations. Subject P3 underwent physical stress with an ergometer on different levels. Subject P4 performed a breathing maneuver during the examination.*

3.2. Right Ventricle Segmentation

The algorithm for segmentation of the RV blood pool (RVBP) relies on the assumption that the target region is a bright, compact area adjacent to the LVM. It successively optimizes an initial estimation of the RVBP towards a coherent segmentation. The algorithm works on an existing segmentation of the LV myocardium and blood pool, which can be obtained by the approaches described by Chitiboi et al. [CHT*14] or Zöhrer et al. [ZHC*17] (Figure 2, left). The image data is separated into individual heart cycles by analyzing the LVBP area curve derived from the LVBP segmentation (Chitiboi et al. [CHT*14]) (Figure 3).

The initial estimation of the RVBP combines two criteria for brightness and proximity to the LVM, assigning each voxel a probability of belonging to the RVBP. Since the RVBP is adjacent to the LVM and blood shows as high intensities in the image data, we derive an intensity interval of interest from the known region. The direct neighbors of the LVM contour (Figure 2, middle) are separated into bright and dark areas using fuzzy C-means clustering (Dunn [Dun73]) (Figure 4, left). The histogram of the bright areas is calculated, and voxels above the third quartile in the histogram are considered to belong to the RVBP (Figure 4, right). Using the third quartile as threshold has been determined experimentally to distinguish the RVBP from surrounding areas. The resulting values are normalized to the interval [0, 1]. We constrain the initial estimation to regions close to the LVM by calculating the Euclidean in-plane distance from the LVM for all voxels. The expected diameter of the RVBP in this direction is in the interval [21, 45] mm in normal adults, and the expected RV wall thickness in the interval [1, 6] mm (Rudski et al. [RLA*10]). We expect the complete RVBP area to be within a distance d_{max} of the LVM. For normal human adults, we set d_{max} to 50 mm, which approximates the combined RVBP diameter and RV wall thickness. This value must be adapted to age, species and disease. The probability of voxels farther away than d_{max} is set to zero, the remaining values are inverted and normalized to the interval [0, 1]. The product of both probabilities produces a combined probability map that contains a first estimate of the RVBP region (Figure 5, left). Because the RVBP may be surrounded by other structures in the same intensity range, such as fat, we identify and remove strong local borders to break up erroneously connected areas by extracting local gradients from the image using a Gaussian kernel with $\sigma_{gradient} = 1mm$, and removing areas with a normalized gradient magnitude above a threshold $t_{gradient} = 0.2$ from the candidate regions. The Gaussian σ is the smallest possible kernel size for the given voxel resolution ($1.6mm$)in the employed Gaussian filter implementation. We determined the threshold empirically by comparing the histograms of all gradient magnitude images and choosing a value that is robustly above the second quartile.

Candidate regions that are not adjacent to the LVM (Figure 2, right) are discarded (Figure 5, middle). The RVBP is located in the vicinity of the liver and other tissue with similar intensity ranges. To prevent leakage across weak gradients into these neighboring regions, we calculate the temporal mean of the RVBP candidate regions and extract the skeleton of this average segmentation to obtain points that are very likely to be in the RVBP. These points are used as input for a watershed segmentation on the combined probability map, where only the largest region on each time point is kept (Figure 5, right). Voxels between the RVBP candidate and the LVM that are in the intensity range of the RV candidate region are added.

The main cause for segmentation leakage are weak gradients between the RVBP and surrounding tissue. The border of the RVBP on the free wall side can be assumed to be smooth and without protruding areas. We exploit this by computing the convex hull of the RVBP candidate and analyzing the areas that are in the convex hull, but not in the candidate region. If the segmentation leaked from the free wall, the convex hull will contain regions that are farther away from the LVBP center than the RVBP candidate center. Frames containing such regions are discarded, and replaced by shape-based interpolation (Herman et al. [HZB92]) between the neighboring time points. The resulting mask is not further constrained by the LVM segmentation, so both regions can partially overlap (Figure 6, left).

3.3. Extraction of Interventricular Septum Motion

On each time point, we connected the gravity centers of the two blood pool segmentations by a line, which was then extended to its intersection with the outer segmentation contours. Landmarks for the free walls and the septum borders were derived by intersecting the line and the inner segmentation contours of LVBP and RVBP (Figure 6, left). This produced four landmarks for each frame: a point on the RV free wall (p_{RVF}), a point on the border between RVBP and IVS (p_{RVS}), a point on the border between IVS and LVBP (p_{LVS}), and a point on the LV free wall (p_{LVF}). From these landmarks, we calculated the following parameters for each time point (extended from Francone et al. [FDK*06]):

$$l_{Heart} = |p_{RVF} - p_{LVF}| \quad (1a)$$

$$l_{LV} = |p_{RVS} - p_{LVF}| \quad (1b)$$

$$l_{Septum} = |p_{RVS} - p_{LVS}| \quad (1c)$$

To obtain parameter values comparable between subjects, we normalized the values to the heart diameter l_{Heart} of the respective time point. We decided against an interactive correction of the landmarks in this step to avoid operator bias effects.

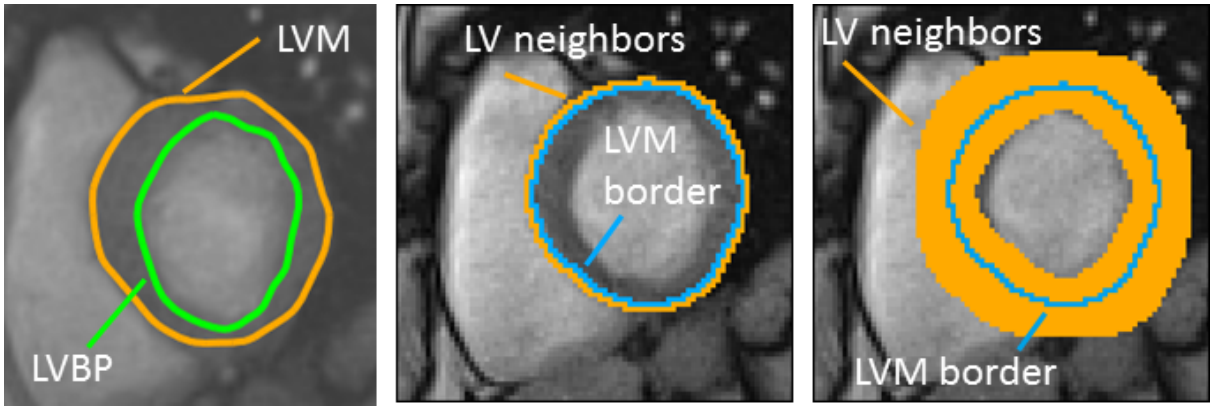

Figure 2: *Left: Image frame with LVM and LVBP contours. Middle: LVM neighborhood for intensity analysis (blue: LVM border for reference, orange: LV neighborhood). Right: LVM neighborhood to connect to RVBP candidate regions (blue: LVM border for reference, orange: LV neighborhood).*

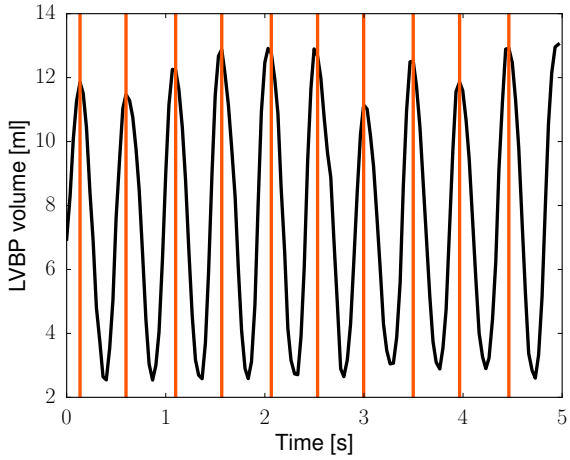

Figure 3: *Cardiac cycle separation based on the LVBP area curve of dataset P3 e. The vertical orange bars indicate time points where complete heart cycles start.*

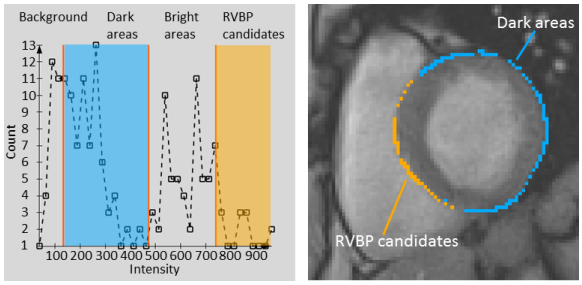

Figure 4: *Left: Histogram for the direct LVM neighbors for a single frame. The vertical orange bars indicate the fuzzy C-means clusters for background, dark areas and bright areas (including RVBP candidates). The intensity range for dark areas is overlayed in blue, the one for RVBP candidates in orange. Right: Classification into RVBP candidate voxels and dark voxels.*

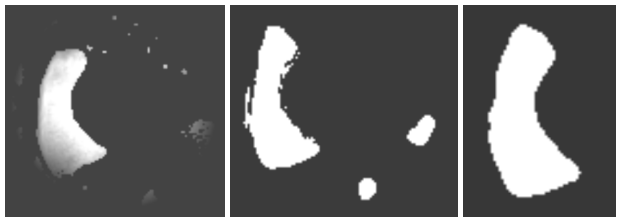

Figure 5: *Left: Combined probability map showing voxels that are at most d_{max} mm away from the LV myocardium and in the intensity range expected for the RVBP. Middle: Intermediate RVBP estimation. Right: RVBP region after watershed segmentation and morphological postprocessing.*

3.4. Estimation of Respiration Phase

To be able to assess the influence of respiration on heart cycles and corresponding parameters, we estimated the breathing phase from the image data. Since the image acquisition slice is fixed, any change in the lung volume is linked to the motion of the diaphragm and ribcage, which indicates the breathing phase. For a coarse lung segmentation, we used a simplified variant of the RVBP segmentation algorithm from above. We calculated the histogram of the dark voxels in the fuzzily-clustered LVM neighborhood (Figure 4). Image voxels that are darker than the minimum intensity in this histogram were considered to be lung voxels. Small regions and regions that were not in the extended neighborhood of the LVM were removed, leaving a single connected region that approximated the lung cavity (Figure 6, right).

We defined the area of this lung segmentation on each frame as the relative inspiration level, and normalized it to the maximum lung segmentation volume of each subject. The inspiration level curve plotted over all time points corresponds to the breathing states. We extracted the respiration cycles by identifying minima and maxima in this curve to connect inspiration and expira-

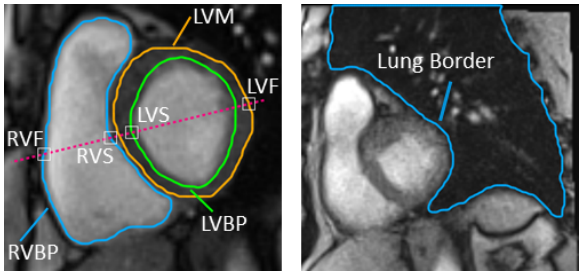

Figure 6: *Left: Contour of RVBP segmentation, with extracted landmarks (RVF: RV free wall, RVS: RV septum border, LVS: LV septum border, LVF: LV free wall) and LVM and LVBP contours for reference. Right: Coarse lung segmentation.*

tion phases. Incomplete respiration cycles were approximated by assuming that they have the length of the average complete cycle (Figure 7). The respiration phase was then defined as the relative index of a frame within a respiration cycle.

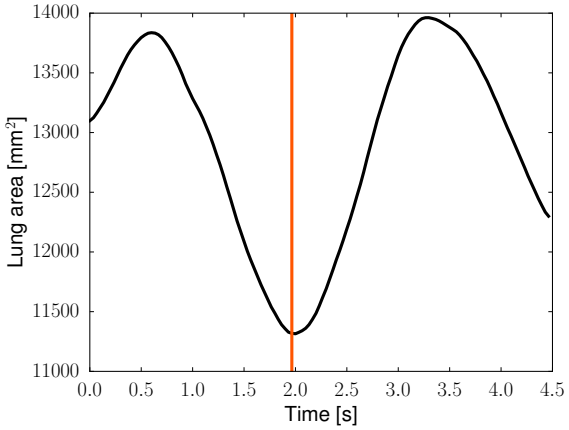

Figure 7: *Respiration cycle separation based on the lung area curve for dataset P3 e. The vertical orange bar indicates the time point where a breathing cycle starts.*

3.5. Exploration Techniques

The resulting parameter data is inherently multi-dimensional. We extracted parameters for every time point in every cycle. Each time point is associated with a cardiac and respiratory phase, and the parameters themselves are physiologically interdependent. Our main focus for this step was to identify techniques to navigate and explore the parameters and the underlying image data. First, we need to define a number of terms:

Cardiac frame index The time point index of a frame within a contraction cycle. The number of image frames in a cycle can vary.

Relative cardiac phase The normalized time point index of a frame in the contraction cycle in the interval [0, 1].

Cycle index The index of a cycle within an image sequence.

Inspiration level The lung area of a frame, normalized over all cases for each subject that show approximately the same slice.

Respiration phase The normalized phase of a frame indicating the respiration state between 0 (expiration) and 1 (inspiration).

The basic concept for exploration is the combination of a parallel coordinates display, a parameter map, a 2D image viewer and a curve plot. Because every image frame is associated with a cardiac frame index and a cycle index, and in turn a relative cardiac phase and a respiration phase, the information displayed in these viewers can be synchronized between these dimensions.

3.6. Parallel Coordinates

The starting point for the parameter exploration is a visualization of parallel coordinates, offering the most abstract view on all derived parameters, including cardiac and respiration phase. The use of parallel coordinates allows to navigate temporal positions (such as cardiac phase), per-frame functional parameters (such as septum thickness) and per-case properties (such as stress level) on the same abstraction level, while a 2D plot or color-encoded parameters would require focusing on a particular subset of parameters. We combined the relative cardiac phase, the respiratory phase, the inspiration level, the heart diameter, the normalized septum thickness, the LVBP diameter and the stress level (in Watt) in an interactive display. By brushing over the lines using the mouse, a subset of time points can be selected. This can be used to examine the association between certain cardiac or respiratory phases and parameter values (Figures 8 and 9), or between high parameter values, phases and stress level (Figure 10). The selection is used to filter the parameter map display to highlight relevant time points (Figure 11). For the exploration of multiple acquisitions of the same subject under different conditions, such as the normal and stress cases of subject P3, the parameters can be combined in a single parallel coordinates display, with per-case displays arranged side-by-side (Figure 12).

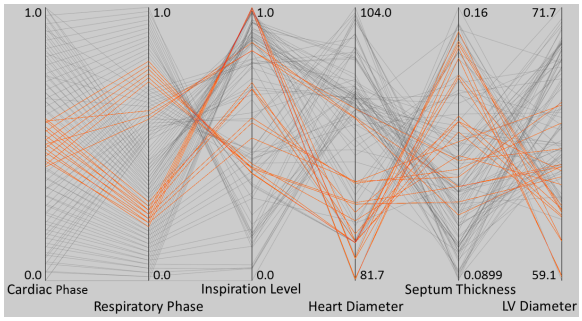

Figure 8: *Parallel coordinates display showing cardiac phase, respiratory phase, inspiration level, heart diameter, septum thickness and LVBP diameter for dataset P3 a (normal). Each polyline connects the respective parameters from one frame. Cardiac phases around end-systole have been selected (orange lines). Note the association with respiratory phases, and the higher variation in heart diameter and relative septum thickness compared to the stress dataset in Figure 9.*

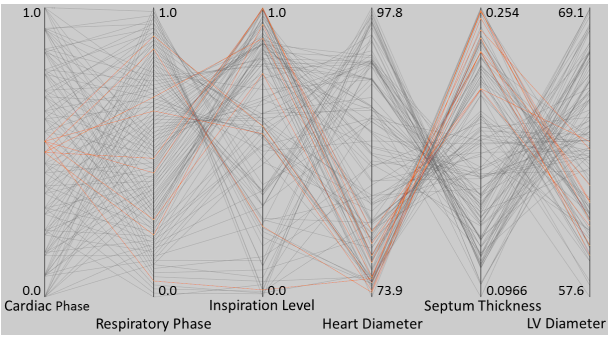

Figure 9: *Parallel coordinates display showing cardiac phase, respiratory phase, inspiration level, heart diameter, septum thickness and LVBP diameter for dataset P3 e (stress at 100W). Cardiac phases around end-systole have been selected (orange lines). Note how respiratory phase and inspiration level vary over the cycles, while heart diameter and septum thickness are comparable.*

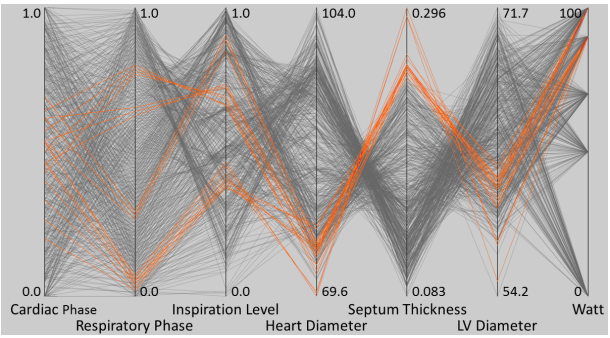

Figure 10: *Parallel coordinates display showing cardiac phase, respiratory phase, inspiration level, heart diameter, septum thickness, LVBP diameter and stress level for all datasets from subject P3. Parameters have been filtered to show only time points with high relative septum thickness (orange lines). Note how this corresponds to high stress levels and increased inspiration levels.*

3.7. Parameter Maps

On the next detail level, one parameter and its dependence on contraction and respiration states is explored. The parameter is plotted as a two-dimensional color-coded map where each map position contains the parameter value for a specific cardiac frame and cycle index. The resulting map allows to visually identify patterns to assess behavior and to qualitatively compare datasets. To aid navigation, positions in the parameter map are linked to the underlying image and a curve plot showing information for all cycles (Figure 11). As the heart cycles differ in length, the map can either be arranged by the frame index, or be resampled to the relative cardiac phase (Figure 14).

The color map used to encode parameter values is important for the interpretation and ease of access to the parameters. We chose a color scheme from ColorBrewer (Brewer [Bre13], Harrower et al. [HB03]) with nine intervals that is scaled to the parameter values.

3.8. Parameter Curves

Once an interesting parameter or dimension has been identified, the information can be presented in a more condensed way. Plotting a parameter over all time points of the original image sequence shows behavior from successive cardiac cycles embedded in the respiratory cycle (Figure 13). By plotting both the cycles and their average, the variation of a parameter over multiple cycles can be assessed (Figure 16). Time points in the curves can be interactively synchronized to the parameter map or the image viewer to allow navigating to time points and cycles of interest. Curves representing a cycle selected in the image viewer or in the parameter map can be highlighted.

4. Results

We performed the automatic analysis steps for all ten datasets, and obtained RV segmentations and landmarks for all time points. From that, we calculated heart diameter, septum thickness (both absolute and normalized) and LVBP diameter (Tables 2, 3, 4 and 5). Two observers explored the datasets using the approaches described above to assess the results and determine how well parameter variation dependent on respiration and stress could be examined. They started in the parallel coordinates view and interactively selected different cardiac phases, respiratory phases and different parameter value ranges to highlight associations between these parameters. The selected time points were highlighted in the parameter map by shading the unselected ones. In the parameter map display, the observers selected different parameters. When the map showed interesting values, such as particularly high or low ones, they clicked on the respective map position, which synchronized the image viewer to the matching image frame and highlighted the respective curve and time point in the curve plot. The curve plot showed curves for all cycles for the same parameter as the parameter map. The observers spent five to ten minutes each for subjects P1 and P2, and fifteen to twenty minutes each for subjects P3 and P4, including the combined analysis of all P3 datasets. They were confident to have grasped relevant characteristics and parameter associations of the respective acquisitions (see Figures 8, 9, 10 and 11 for selected exploration steps).

Dataset	Min; max	Mean $\pm$ SD
P1 a	95.11; 102.52	99.46 $\pm$ 1.80
P1 b	95.88; 101.47	99.10 $\pm$ 1.50
P2 a	91.88; 112.27	103.60 $\pm$ 5.38
P2 b	92.83; 112.03	104.25 $\pm$ 5.11
P3 a	81.62; 102.65	92.76 $\pm$ 5.72
P3 b	76.25; 100.07	88.50 $\pm$ 7.51
P3 c	74.52; 102.22	88.35 $\pm$ 7.89
P3 d	74.02; 100.33	87.11 $\pm$ 8.76
P3 e	72.13; 97.60	85.19 $\pm$ 8.04
P4	70.81; 94.04	84.25 $\pm$ 3.86

Table 2: *Heart diameter over all cycles [mm].*

The right ventricle segmentations were reviewed by the observers, with the possibility to manually correct the result. The RVBP segmentation was missing parts of the lower RVBP in

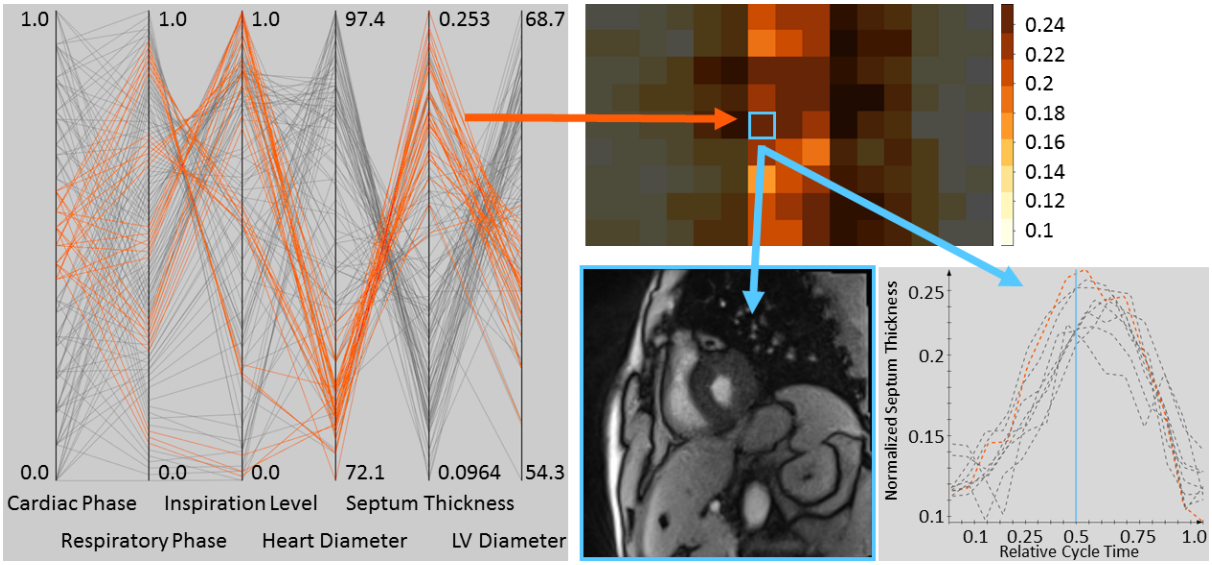

Figure 11: *Example for synchronized viewers, showing dataset P3 e. In the parallel coordinates display (left), cardiac phases around end-systole have been selected (orange lines). All other time points are displayed shaded in the parameter map display (upper right), where a time point with a particularly high septum thickness has been selected (blue rectangle). The corresponding image has been loaded in the image display (bottom middle), and the cycle containing the selected time point has been highlighted (blue curve) in the curve plot showing all cycles (bottom right). The time points show different respiration phases and inspiration levels, but consistently small heart diameters and high relative septum thickness, indicating increased breathing and increased contraction under stress.*

Dataset	Min; max	Mean ± SD
P1 a	6.10; 12.90	9.07 ± 1.22
P1 b	6.57; 12.41	8.93 ± 1.22
P2 a	5.91; 11.27	8.96 ± 1.15
P2 b	6.33; 12.09	9.30 ± 1.08
P3 a	7.31; 14.46	11.29 ± 1.45
P3 b	7.30; 16.68	12.69 ± 1.93
P3 c	8.74; 18.98	14.04 ± 2.61
P3 d	8.48; 18.53	13.89 ± 2.55
P3 e	8.84; 19.05	14.15 ± 2.54
P4	6.43; 17.88	9.61 ± 1.64

Table 3: *Absolute septum thickness over all cycles [mm].*

Dataset	Min; max	Mean ± SD
P1 a	0.06; 0.13	0.09 ± 0.01
P1 b	0.07; 0.13	0.09 ± 0.01
P2 a	0.05; 0.12	0.09 ± 0.01
P2 b	0.06; 0.12	0.09 ± 0.01
P3 a	0.08; 0.17	0.12 ± 0.02
P3 b	0.08; 0.22	0.15 ± 0.03
P3 c	0.09; 0.24	0.16 ± 0.04
P3 d	0.09; 0.24	0.16 ± 0.04
P3 e	0.10; 0.25	0.17 ± 0.04
P4	0.07; 0.21	0.11 ± 0.02

Table 4: *Normalized septum thickness over all cycles.*

Dataset	Min; max	Mean ± SD
P1 a	0.60; 0.70	0.66 ± 0.03
P1 b	0.60; 0.71	0.66 ± 0.02
P2 a	0.62; 0.71	0.66 ± 0.02
P2 b	0.62; 0.73	0.66 ± 0.02
P3 a	0.64; 0.78	0.72 ± 0.03
P3 b	0.67; 0.81	0.74 ± 0.03
P3 c	0.65; 0.83	0.73 ± 0.05
P3 d	0.65; 0.83	0.74 ± 0.05
P3 e	0.67; 0.81	0.74 ± 0.04
P4	0.63; 0.84	0.73 ± 0.04

Table 5: *Normalized LV bloodpool diameter over all cycles.*

399 out of 2321 image frames (17%) where the intensity distribution within the blood pool was inhomogeneous. Neither observer chose to correct the segmentations. Segmentation time was $22.24 \pm 20.93s$ per dataset.

For multiple similar acquisitions of the same subject, the agreement of the calculated parameter values was good. Measured average heart diameter differed by 0.4% between acquisitions for (subject P1) and by 0.6% for subject P2. Average septum thickness differed by 1.5% (P1) and 3.8% (P2). Average normalized septum thickness was equal within two significant figures. Absolute differences in minimum, average and maximum values were smaller than the in-plane resolution for all parameters. The change in standard deviation for the average septum thickness was 0% for P1 and 6.1% for P2.

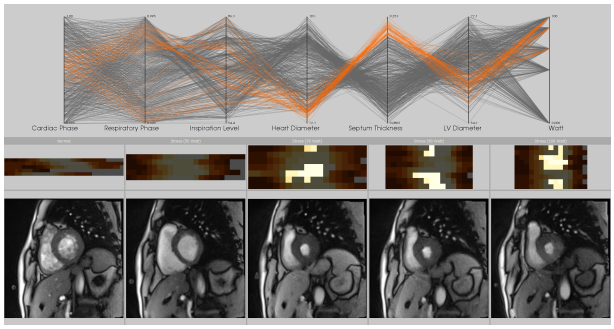

Figure 12: *Parallel coordinates display, parameter map displays and image displays arranged to explore several datasets simultaneously. The parallel coordinate display shows all parameters (cf. Fig. 10) for all datasets from subject P3. The parameter maps show the septum thickness values for each stress level, and the image displays show a selected time point from each dataset. In the parallel coordinates, polylines with a high normalized septum thickness have been selected, and the corresponding time points in the parameter maps are highlighted. Note how only datasets P3 c, d and e contain time points with septum thickness in the selected value range. From the parameter maps of these datasets, time points with very large septum thickness have been selected, which are shown in the image displays at the bottom. Note the similar appearance and the different respiration phases of the slices.*

In the datasets of subject P3 acquired under normal conditions (P3 a) and different levels of physical stress (P3 b-P3 e), average septum thickness increased from 11.29*mm* in normal state to 12.69*mm* on the lowest stress level and to 14.15*mm* on the highest stress level, corresponding to changes of 12.4% and 25.3%. The change in standard deviation for the average septum thickness from the normal state was 34.3% to the lowest stress level and 135% to the highest stress level.

5. Discussion

The observers had minimal interaction effort during segmentation and landmark extraction, as no corrections were required. They could use the exploration approach successfully to see associations between cardiac and respiratory phases and motion parameters, in particular using the parallel coordinates view. Synchronization of the viewers was considered helpful by the observers to identify where particularly low or high values occurred. They noted the visual access to the changes in respiration and septum thickness associated with stress levels (see Figures 8, 9, 10 and 17). We plan to conduct a user study involving more observers and more cases to validate the usability of our approach.

The analysis of subjects P1 and P2 suggests that our approach can robustly quantify septum motion. Through-plane motion caused by changes in breathing distorts the parameter values, but shows as increased variation in our analysis.

Because the measurements are derived from only a few landmarks, consistency of the underlying segmentations is important. Our segmentation approach missed parts in the lower half of the RVBP in some frames..The observers visually inspected the segmentation results and were to manually correct a segmentation when it did not cover the middle of the IVS or the middle of the RV free wall. No corrections were made, introducing additional variation due to wrong landmarks. We will examine the influence of RVBP segmentation quality in future work. Given the promising right ventricle segmentation results that have been published using deep-learning-based approaches for conventional MRI data, it would be interesting to apply a deep learning approach to real-time MRI data. In addition, it would be interesting to increase the number of landmarks to create multiple lines crossing the IVS to obtain more robust parameter values.

In the parameter maps, we used a single color map for all parameters that was scaled relative to the value range. Thresholds for normal and pathological values could be integrated into the color maps for specific parameters, which would likely support interpretation of the visualization.

In our analysis, we focused on the septum thickness, the heart diameter and the LV bloodpool diameter. The approach could be extended to include other measurements for function assessment, such as IVS shape, LVBP area, or myocardial mass. Since the synchronization of the viewers is centered on cardiac and respiratory phases, multi-slice acquisitions could be processed and explored as well. Comparative exploration of multiple patient groups, for example patients with arrhythmia against healthy subjects, could be realized by the multi-dataset approach shown in Figure 12.

6. Conclusion

This work proposes an automatic approach for the quantification of septum motion from real-time cardiac MRI in a short-axis orientation, and a concept to explore the results of this analysis. The approach provides access to the assessment of variation in relative septum thickness caused by factors such as physical stress and changes in respiration. Analyzing repeated measurements produced comparable results, while physiological changes produced increased variation in the parameters. The exploration concept provides the means for an interactive inspection of the influence of breathing and physical stress on cardiac contraction. In future work, this will be integrated in a clinically applicable solution for studies on the variation of cardiac function.

References

[AABW12] ANDRIENKO G., ANDRIENKO N., BURCH M., WEISKOPF D.: Visual analytics methodology for eye movement studies. *Visualization and Computer Graphics, IEEE Transactions on 18*, 12 (Dec 2012), 2889–2898. 2

[Bre02] BREEUWER M.: Comprehensive visualization of first-pass myocardial perfusion: The uptake movie and the perfusogram. In *Proc. of the International Society for Magnetic Resonance in Medicine, 10th Scientific Meeting* (2002). 2

[Bre13] BREWER C. A.: ColorBrewer. http://www.ColorBrewer.org, 2013. [Online; accessed 26-June-2017]. 6

[CHT*14] CHITIBOI T., HENNEMUTH A., TAUTZ L., HUELLEBRAND M., FRAHM J., LINSEN L., HAHN H.: Context-based segmentation and analysis of multi-cycle real-time cardiac MRI. In *Biomedical Imaging (ISBI), 2014 IEEE 11th International Symposium on* (2014), IEEE, pp. 943–946. 2, 3

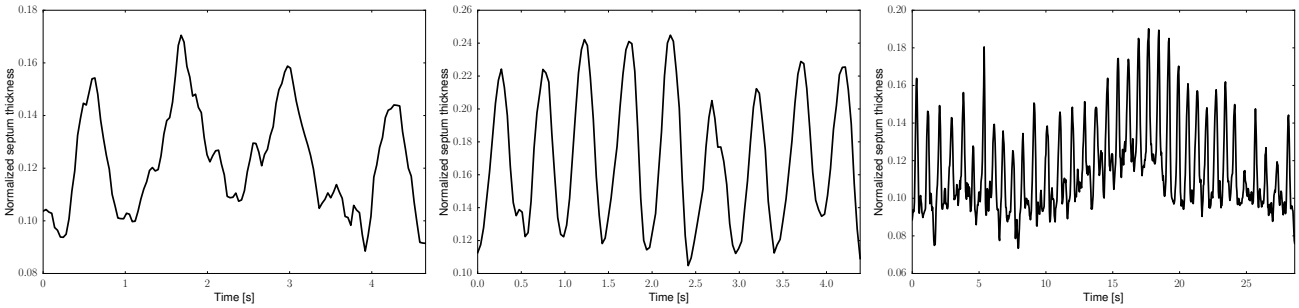

Figure 13: *Normalized septum thickness over all time points. Note the effect of change in stress and in particular respiration on the septum (Left: dataset P3 a (normal), middle: P3 e (Stress 100W), right: P4 (Valsalva)).*

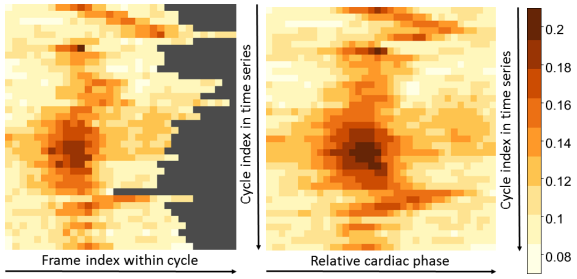

Figure 14: *Normalized septum thickness over dataset P4 cycles, aligned by cardiac frame index (left) and resampled to relative cardiac phase (right). Light colors indicate low values, dark colors high values. The subject performed a breathing maneuver with a phase of enhanced pressure. Septum thickness varies strongly during systolic cardiac phase over the cycles. Note how the variation in cycle lengths distorts the map when aligned by cardiac frame index.*

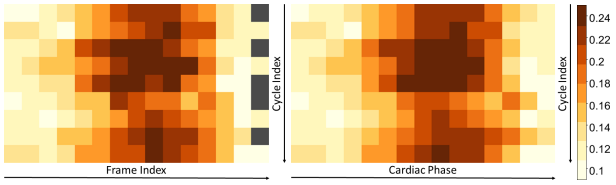

Figure 15: *Normalized septum thickness over dataset P3 e cycles, aligned by cardiac frame index (top) and resampled to relative cardiac phase (bottom). Light colors indicate low values, dark colors high values. Septum thickness varies over the cycles, but the variation is less pronounced in comparison to the Valsalva cycles in Figure 14.*

[CHT*15] CHITIBOI T., HENNEMUTH A., TAUTZ L., HUELLEBRAND M., FRAHM J., HAHN H.: Automatic multi-cycle analysis of cardiac function from real-time MRI. *Journal of Cardiovascular Magnetic Resonance 17*, 1 (2015), P385. 2

[CRF*17] CHITIBOI T., RAMB R., FENG L., PIEKARSKI E., TAUTZ L., HENNEMUTH A., AXEL L.: Multi-cycle Reconstruction of Cardiac MRI for the Analysis of Inter-ventricular Septum Motion During Free Breathing. In *Functional Imaging and Modelling of the Heart*, Pop M., Wright G. A., (Eds.), vol. 10263. 2017, pp. 63–72. 2

[DDH*71] DIAMOND M. A., DILLON J. C., HAINE C. L., CHANG S., FEIGENBAUM H.: Echocardiographic features of atrial septal defect. *Circulation 43*, 1 (1971), 129–135. 1

[Dun73] DUNN J. C.: A Fuzzy Relative of the ISODATA Process and Its Use in Detecting Compact Well-Separated Clusters. *Journal of Cybernetics 3*, 3 (1973), 32–57. 3

[FAC*16] FENG L., AXEL L., CHANDARANA H., BLOCK K. T., SODICKSON D. K., OTAZO R.: XD-GRASP: Golden-angle radial MRI with reconstruction of extra motion-state dimensions using compressed sensing: XD-GRASP: Extra-Dimensional Golden-angle Radial Sparse Parallel MRI. *Magnetic Resonance in Medicine 75*, 2 (Feb. 2016), 775–788. 2

[FDK*06] FRANCONE M., DYMARKOWSKI S., KALANTZI M., RADEMAKERS F. E., BOGAERT J.: Assessment of ventricular coupling with real-time cine MRI and its value to differentiate constrictive pericarditis from restrictive cardiomyopathy. *European Radiology 16*, 4 (Apr. 2006), 944–951. 3

[FDKB05] FRANCONE M., DYMARKOWSKI S., KALANTZI M., BOGAERT J.: Real-time cine MRI of ventricular septal motion: A novel approach to assess ventricular coupling. *Journal of Magnetic Resonance Imaging 21*, 3 (Mar. 2005), 305–309. 2

[GKS57] GORLIN R., KNOWLES J. H., STOREY C. F.: The Valsalva maneuver as a test of cardiac function: pathologic physiology and clinical significance. *The American Journal of Medicine 22*, 2 (1957), 197–212. 2

[HB03] HARROWER M., BREWER C. A.: ColorBrewer.org: An Online Tool for Selecting Colour Schemes for Maps. *The Cartographic Journal 40*, 1 (June 2003), 27–37. 6

[HZB92] HERMAN G. T., ZHENG J., BUCHOLTZ C. A.: Shape-based interpolation. *IEEE Computer Graphics and Applications 12*, 3 (May 1992), 69–79. 3

[Ins85] INSELBERG A.: The plane with parallel coordinates. *The Visual Computer 1*, 2 (1985), 69–91. 2

[LAW*16] LUO G., AN R., WANG K., DONG S., ZHANG H.: A deep learning network for right ventricle segmentation in short-axis MRI. In *Computing in Cardiology Conference (CinC), 2016* (2016), IEEE, pp. 485–488. 2

[ODH*07] OELTZE S., DOLEISCH H., HAUSER H., MUIGG P., PREIM B.: Interactive visual analysis of perfusion data. *IEEE Transactions on Visualization and Computer Graphics 13*, 6 (2007), 1392–1399. 2

[PD11] PETITJEAN C., DACHER J.-N.: A review of segmentation methods in short axis cardiac MR images. *Medical image analysis 15*, 2 (2011), 169–184. 2

[POM*09] PREIM B., OELTZE S., MLEJNEK M., GROELLER E., HENNEMUTH A., BEHRENS S.: Survey of the Visual Exploration and Analy-

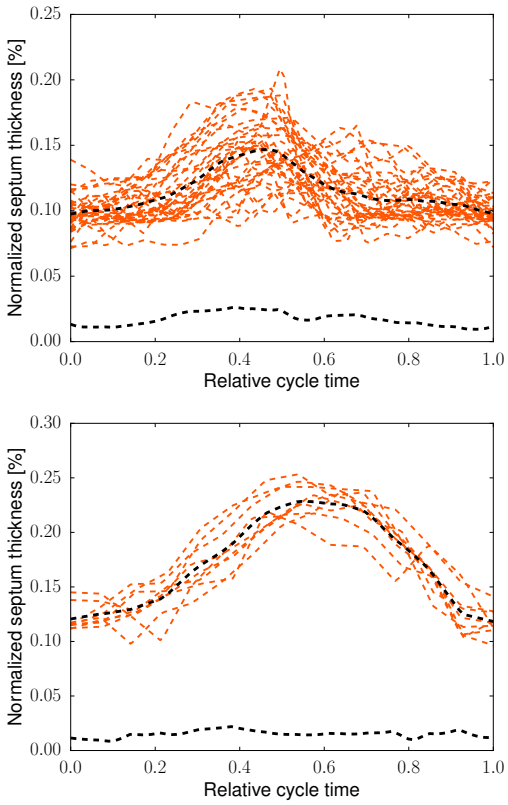

Figure 16: *Normalized septum thickness per cycle (orange: cycle curves, black: average and standard deviation over cycles). Top: Dataset P4, where the subject performed a breathing maneuver during image acquisition, which changes pressure in the left ventricle. Note the high variation between the cycles, in particular during systole. Bottom: Dataset P3 e, where the subject was imaged on a high stress level. Note how the septum thickness changes strongly during the heart cycles, but variation between the cycles is less pronounced.*

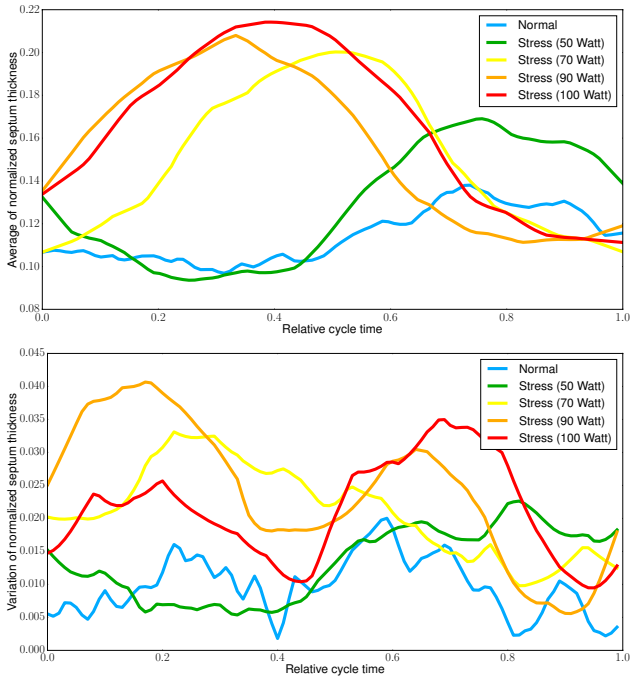

Figure 17: *Normalized septum thickness in different stress acquisitions. The curves are color-coded from blue (normal) to red (highest stress). Note the changes in average thickness (top) and the increase in variation (bottom) for higher stress levels.*

sis of Perfusion Data. *IEEE Transactions on Visualization and Computer Graphics 15*, 2 (Mar. 2009), 205–220. 2

[PZB*15] PETITJEAN C., ZULUAGA M. A., BAI W., DACHER J.-N., GROSGEORGE D., CAUDRON J., RUAN S., AYED I. B., CARDOSO M. J., CHEN H.-C., OTHERS: Right ventricle segmentation from cardiac MRI: a collation study. *Medical image analysis 19*, 1 (2015), 187–202. 2

[RLA*10] RUDSKI L. G., LAI W. W., AFILALO J., HUA L., HANDSCHUMACHER M. D., CHANDRASEKARAN K., SOLOMON S. D., LOUIE E. K., SCHILLER N. B.: Guidelines for the Echocardiographic Assessment of the Right Heart in Adults: A Report from the American Society of Echocardiography. *Journal of the American Society of Echocardiography 23*, 7 (July 2010), 685–713. 3

[RMF*05] ROELEVELD R. J., MARCUS J. T., FAES T. J. C., GAN T.-J., BOONSTRA A., POSTMUS P. E., VONK-NOORDEGRAAF A.: Interventricular Septal Configuration at MR Imaging and Pulmonary Arterial Pressure in Pulmonary Hypertension. *Radiology 234*, 3 (Mar. 2005), 710–717. 1

[TFO*16a] TAUTZ L., FENG L., OTAZO R., HENNEMUTH A., AXEL L.: Analysis of cardiac interventricular septum motion in different respiratory states. In *Medical Imaging 2016: Biomedical Applications in Molecular, Structural, and Functional Imaging* (Mar. 2016), p. 97880X. 2

[TFO*16b] TAUTZ L., FENG L., OTAZO R., HENNEMUTH A., AXEL L.: Cardiac function analysis with cardiorespiratory-synchronized CMR. *Journal of Cardiovascular Magnetic Resonance 18*, Suppl 1 (2016), W24. 2

[Tra16] TRAN P. V.: A Fully Convolutional Neural Network for Cardiac Segmentation in Short-Axis MRI. *ArXiv e-prints* (Apr. 2016). 2

[UZV*10] UECKER M., ZHANG S., VOIT D., KARAUS A., MERBOLDT K.-D., FRAHM J.: Real-time MRI at a resolution of 20 ms. *NMR in Biomedicine 23*, 8 (Oct. 2010), 986–994. 1, 2

[VFR*12] VINEGONI C., FERUGLIO P. F., RAZANSKY D., GORBATOV R., NTZIACHRISTOS V., SBARBATI A., NAHRENDORF M., WEISSLEDER R.: Mapping molecular agents distributions in whole mice hearts using born-normalized optical projection tomography. *PLoS ONE 7*, 4 (04 2012), e34427. 2

[WML*17] WANG K., MA Y., LEI R., YANG Z., MA Y.: Automatic right ventricle segmentation in cardiac MRI via anisotropic diffusion and SPCNN. In *Proc. SPIE* (Feb. 2017), Wang Y., Pham T. D., Vozenilek V., Zhang D., Xie Y., (Eds.), p. 1022527. 2

[ZCG85] ZEE-CHENG C. S., GIBBS H. R.: Paradoxical ventricular septal motion with right ventricular dilatation as a manifestation of pure pressure overload due to pulmonary veno-occlusive disease. *Clinical Cardiology 8*, 11 (1985), 603–606. 1

[ZHC*17] ZOEHRER F., HUELLEBRAND M., CHITIBOI T., OECHTERING T., SIEREN M., FRAHM J., HAHN H. K., HENNEMUTH A.: Real-time myocardium segmentation for the assessment of cardiac function variation. In *Proc. SPIE* (2017), vol. 10137, pp. 101370L–101370L–7. 2, 3